PHYSICAL REVIEW FLUIDS **10**, 034801 (2025)

Ship waves on an elastic floating ice plate

Sergei Badulin [*,†]
Skolkovo Institute of Science and Technology, Bolshoy Boulevard 30, Building 1, 121205 Moscow, Russia

Vladimir Gnevyshev [‡]
P.P. Shirshov Institute of Oceanology of the Russian Academy of Sciences, 36 Nakhimovsky Avenue, 117997 Moscow, Russia

Yury Stepanyants [¶,§]
Department of Applied Mathematics, Nizhny Novgorod State Technical University, n.a. R.E. Alekseev, 24 Minin Street, 603950 Nizhny Novgorod, Russia

(Received 16 October 2024; accepted 17 January 2025; published 4 March 2025)

We study a wave wake produced by a finite-size source uniformly moving on an ice plate overlying deep water. We describe the kinematic characteristics of source-generated flexural-gravity waves in terms of isophase patterns scaled by the minimum phase speed and show that the wave picture is determined by ad hoc defined Mach and Bond numbers. Then, we show that several bifurcations occur in the wave wake when the source speed increases. In particular, cusps appear in the wake patterns at certain speeds due to the merging at specific points of two or three wave characteristics (wave rays) which correspond to longitudinal (divergent), transverse, and fan waves. To describe the distribution of wave amplitudes in the wake accounting for the source size and shape, we use the reference solution approach. This approach agrees with the stationary phase method in the far-field zone and reproduces also specific wave dynamics at short and intermediate distances from the source. The effect of a source shape on the wave wake pattern is graphically illustrated for the elliptic source as the dependence on the dimensionless Bond number and the source length-to-beam ratio. The illustrations of the source speed and shape effects are given for low-speed regimes when wave patterns are conformed by single-ray solutions. Ways of the generalization of the suggested approach are outlined.

DOI: 10.1103/PhysRevFluids.10.034801

I. INTRODUCTION

The classic problem of ship waves, i.e., stationary waves generated by a moving source on a water surface (or more generally, in an isotropic dispersive media), was formulated for the first time, apparently, by Thomson [1] (Lord Kelvin after 1892). Since that time, Kelvin's approach was further developed, applied to waves in various media, and presented in many classical textbooks (see, for example, Refs. [2–5]). Nowadays, there is a great interest in the study of ship-type waves

[*]Also at P.P. Shirshov Institute of Oceanology of the Russian Academy of Sciences, 36 Nakhimovsky Avenue, 117997 Moscow, Russia.
[†]Contact author: badulin.si@ocean.ru
[‡]Contact author: avi9783608@gmail.com
[¶]Contact author: yury.stepanyants@unisq.edu.au
[§]Also at University of Southern Queensland, West Street, Toowoomba, Queensland 4350, Australia.

in a ice covered fluid. The interest is dictated by the growing development of marine and ocean resources, including in the polar regions. This requires the development of infrastructure on ice sheets, including airfields and roads for cars, lorries, air-cushion vehicles, snowmobiles, and other motorized vehicles. Therefore, the specific problem of ship-type waves generated on ice plates by a moving load becomes very topical. A similar problem is topical for the artificial very long floating constructions that are used as the airfields [6].

The problem of flexural-gravity waves (FGWs) generation by moving objects on ice sheets floating over the water was considered by many authors (see, for example, Refs. [7–15]). Both stationary and nonstationary problems were considered for the compressed and noncompressed ice. Dispersion properties of free FGWs per se are very well known as a key mechanism of the wave wake formation (see, e.g., Refs. [9,10,12,16] and references therein). The kinematics of FGWs generated by periodic and pulse-type perturbations were also studied both for the uniform and nonuniform ice compression [9,11,14–16].

The typical approach to the investigation of a wave pattern produced by a moving load of finite size in the linear approximation is to present a wave field through the Fourier transform and then, to consider the asymptotics of corresponding integrals in the far zone (see, e.g., Refs. [2–5,12,17]). Such asymptotic approaches (including geometric optics, stationary phase method, steepest descent methods, etc.) are associated with the description of wave propagation along characteristics (rays) and, thus, have certain restrictions and drawbacks. These methods do not allow one to investigate a wave field in the zones close to sources at distances comparable with the characteristic wavelength and source size. Additionally, they produce singularities at caustics, i.e., at the lines or surfaces which are envelopes of ray bunches. In the ship-wave problem, two or more rays can merge at caustics forming cusps. Special approaches are applied to construct approximate regular solutions near the caustics and then, to match them with asymptotic solutions in the far zone (see, e.g., Ref. [4] and references therein). The Airy function represents an example of a regular solution near the caustics that appear in many studies of wave propagation. In the problem of ship wave generation, we meet with the caustics that appear near the so-called Kelvin wedge that conditionally separates the domains of stationary wave wake and a shadow zone where stationary wave disturbances do not exist.

In this paper, we apply an alternative the reference solution approach (RSA) to the description of the wave field generated by a uniformly moving source of finite size on the elastic plate floating on the water surface. It is based on the modulated Gaussian pulses [18–20] as reference functions for tracing the dynamics of spectrally narrow wave packets. The RSA provides the same solution in the far-field zone as the standard stationary phase method (SPM). However, it captures some additional features of the wave dynamics at the intermediate distances from the source [21] as well as in the vicinity of wave caustics. This allows one to avoid inherent singularities in the SPM and get explicit analytical expressions in terms of elementary functions. The solutions obtained can be treated as the result of wave dispersion and linear superposition of different families of solutions located on different rays.

Wave dispersion plays a key role in phase and amplitude distributions of the ship-type wave wake patterns. The existence of the Kelvin wedge for waves of negative dispersion (when the group velocity is decreasing function of a wave number) gives a remarkable example of how the difference of phase and group velocities can confine the wave wake interior. In particular, for deep-water wave dispersion $\omega = \sqrt{g|\mathbf{k}|}$ ($\mathbf{k}$ is a wave vector, ω is a wave frequency, and g is the gravity acceleration) and for more general arbitrary power-type dispersion $\omega \sim |\mathbf{k}|^{-d}$ ($d < 1$), the Kelvin wedge angle does not depend on the source speed. The classic Kelvin wedge angle, $\theta_K \approx 19.5^\circ$, is fully determined by the ratio of the phase and group speeds. This remarkable result can be regarded as a degeneration of models where there are no inherent characteristic physical scales. An alternative extreme case of degeneration for the scale-invariant media is a wave wake in nondispersive media such as a wake formed by acoustic waves in a compressible gas. The identity of the phase and group velocities leads to the collapsing of a wave wake and a singularity appearance on the Mach cone, determined by the ratio of the source velocity to the sound speed (i.e., by the Mach number).

The role of wave dispersion illustrated by the above extreme examples of dispersive and nondispersive wave wakes can be consistently analyzed for waves with a complex dispersion like in the well-known gravity-capillary waves (GCW). It turns out, that the effects of the dimensionless "internal" ratio of the group to phase speeds and the "external" Mach ratio of the source speed to the speed of long waves in the case of a finite-depth fluid are closely linked in this more general case as demonstrated in Refs. [20,22–26]. The characteristic Mach angles are associated with the minima of the phase and group velocities and determine peculiarities of the wave wake interior. These manifestations of wave dispersion are complemented by the interference of different wave systems when the stationarity condition of a wave wake possesses more than one solution for the wavelength. In the case of gravity waves in deep water, there are two families of transverse and divergent waves with the corresponding cusps at the Kelvin angle where two solutions of the stationarity condition coincide.

A wave wake looks more complex for GCWs. For these waves, the dispersion changes its sign at a certain wave scale which leads to the diversity of kinematic and dynamic effects. For GCWs on a water surface, the corresponding scales are small consisting 1.73 cm for the minimum of phase velocity and 2.54 cm for the minimum of group velocity. Rayleigh [27] analyzed the kinematics of one-dimensional pure capillary waves (i.e., waves of positive dispersion) to build a solution of a permanent form. Then he tried to extend this solution to the two-dimensional case with a rather sophisticated geometrical approach. Kelvin [1] was the first who applied the concept of group velocity introduced by Stokes [28] to trace isophase patterns of deep water gravity waves which are waves of negative dispersion. His approach was used further in many publications for different types of waves (see Refs. [3,26] for review). Crapper [29] developed this approach for the analysis of GCWs, i.e., for waves where negative and positive dispersions coexist and provide essential physical effects. Crapper analyzed the wave kinematics both within the ray equations and using the geometry of isophase curves.

The problem of FGWs generation by a moving source is qualitatively similar to the previously studied problem of GCWs generation but has some specifics and practical applications. For this kind of waves, the dispersion changes its sign at much bigger scales in a wide range of tens-hundreds meters depending on the ice cover parameters. This makes the problem of FGW excitation practical and motivates us to draw more attention to details of effects based on real parameters of the floating ice. As aforementioned, the problem was tackled by many authors. In particular, Davys *et al.* [7] (see also Ref. [12]) linked the problem of FGW generation with the general problem of stationary wave wakes and provided quantitative estimates of FGW parameters in the infinitely deep and finite-depth water. The analysis undertaken in these papers was presented in the dimensional form for the particular values of ice plate thickness $h = 2.5$ m and three typical load speeds $U = 30$ m/s, 37.5 m/s, and 50 m/s. Below we present the analysis of the problem in the dimensionless form which allows us to take into account all governing parameters and find critical values of Mach numbers $M = 1, 1.176, 1.417, 1.75$ when wake patterns experience qualitative changes. Using relations between dimensional and nondimensional variables, one can obtain critical parameters for different regimes in dimensional variables.

In the recent publication [30], the authors studied in the linear approximation wave motions produced by a point source pulsating and moving at a constant speed in water parallel to a semi-infinite uncompressed ice sheet. The Green function was derived in the dimensionless variables through the Fourier transform along the direction of forward speed and by the Wiener–Hopf technique along the transverse direction across both the free water surface and ice sheet. A wave motion on a compressed ice sheet generated by a point dipole moving and oscillating in water underneath of an ice plate was also studied in the linear approximation in Ref. [31] using the Fourier transform on spatial coordinates and Laplace transform on time.

The problem of wave generation on an ice sheet by a finite-size (rectangular) source was studied in the linear approximation by Milinazzo *et al.* [32] for a finite-depth fluid. The ice sheet deflection was expressed through the Fourier integral that was evaluated numerically. Asymptotic estimates of the integral was also given for the far-field zone assuming that the aspect ratio of the rectangular load is large. It was demonstrated that the far-field approximation provides a good description of the sheet deflection at distances greater than about one or two wavelengths away from the source. Calculations showed a significant dependence of the amplitude of the ice deflection on the aspect ratio of the load. In our paper we also consider wave motion on an ice sheet generated by a finite-size source of a Gaussian shape with various aspect ratios. We assume for simplicity that the water depth is infinite. The main novelty of our paper is in the suggestion of the reference solution approach to the description of a wave wake generated by a moving source of a finite size in all directions. This allows one to find a wave structure not only in the asymptotic, but at all distances from the source and avoid singularities in the solution.

The rest of the paper is organized as follows. In Sec. II, we present the problem statement and the general analysis of the problem. Kinematics of the flexural-gravity wave wake is presented in Sec. III. Here we inevitably forced to reproduce some known results to match them with the suggested reference solution approach. Then, in Sec. IV, we describe reference solutions in application to flexural-gravity ship wake and find wave amplitude distribution on an ice plate. The results obtained for the uncompressed ice plate floating on the surface of a deep ocean are illustrated graphically. In the Conclusion, we summarize the results obtained and discuss perspectives.

II. PROBLEM STATEMENT AND THE GENERAL ANALYSIS

A. Basic equations

We consider a thin elastic ice plate of a constant thickness and density which is infinite in the horizontal plane and floats on the surface of a perfect incompressible fluid of infinite depth. It is assumed that the pressure disturbance produced by an external load moves rectilinearly at a constant speed U along the horizontal x axis. The problem is studied in the comoving coordinate frame x, y, z, where x and y are the horizontal axes and z is the vertical axis directed upward. The fluid flow is assumed to be potential and the fluid velocity, as well as the ice plate deflection, are relatively small so that the basic set of hydrodynamic equations can be linearized.

The solution for the ice plate deflection can be obtained through the solution of the Laplace equation for the velocity potential $\phi(x, y, z, t)$ which provides the traditional expression for the fluid velocity $\mathbf{u} = \nabla\phi$ [12]:

$$\Delta_\perp\phi + \frac{\partial^2\phi}{\partial z^2} = 0, \quad (|x|, |y| < \infty, \ -\infty \leqslant z \leqslant 0), \quad \Delta_\perp = \frac{\partial^2}{\partial x^2} + \frac{\partial^2}{\partial y^2}. \tag{1}$$

Then, we assume that the lower boundary of the ice plate is always in contact with water, and ice-plate inertia can be neglected (the latter assumption is usually supported by the results of many publications (see, e.g., Ref. [31] and references therein). Denoting the vertical deflection of the ice plate from the undisturbed position by $w(x, y, t)$, we present the kinematic and dynamic boundary conditions at $z = 0$ as

$$\frac{\partial w}{\partial t} + U\frac{\partial w}{\partial x} = \frac{\partial\phi}{\partial z}, \tag{2}$$

$$D\Delta_\perp w + \rho g w + \rho\left(\frac{\partial\phi}{\partial t} + U\frac{\partial\phi}{\partial x}\right) = -P(x, y, t), \tag{3}$$

where $D = Eh^3/[12(1-\nu^2)]$, E is the Young modulus of elastic plate, ν is the Poisson ratio, ρ is the water density, h is the thickness of the ice plate. The first term in Eq. (3) describes the elastic property of the ice plate; two other terms in the left-hand side represent pressure on the surface for small-amplitude potential oscillations of a fluid covered by ice, and $P(x, y, t)$ represents the external pressure. All perturbations generated on the water surface vanish when $z \to -\infty$; in particular, for the vertical component of fluid velocity we have

$$\frac{\partial\phi}{\partial z} \to 0, \quad z \to -\infty. \tag{4}$$

For free infinitesimal perturbations when $P(x, y, t) \equiv 0$, and the variables w and ϕ are proportional to $\exp[\mathrm{i}(\omega t - k_x x - k_y y)]$, we obtain from Eqs. (1)–(4) the dispersion relation (see, for example, Ref. [7]):

$$\omega(k_x, k_y) = U k_x + \sqrt{g|\mathbf{k}| + D|\mathbf{k}|^5/\rho}, \quad |\mathbf{k}|^2 \equiv k^2 = k_x^2 + k_y^2. \tag{5}$$

Using this dispersion relation, one can present a solution of the linear problem through the Fourier integral [2–5,12]:

$$\phi(x, y, t) = \iint A(k_x, k_y) \exp[\mathrm{i}(\omega(k_x, k_y)t - k_x x - k_y y)] dk_x dk_y. \tag{6}$$

The integrals can be evaluated numerically and investigated asymptotically using, for example, the SPM. The detailed comparison of exact and approximated integral evaluation can be found, in particular, in the papers [21,30,32]. In this work we focus on the analytical approach. Below we analyze the dispersion relation in the dimensionless variables and introduce parameters that characterise a wake produced by a moving object.

B. Dimensional analysis: Phase and group Mach numbers

The intrinsic wave frequency in the absence of a current ($U \equiv 0$) depends on the joint effect of gravity and flexural force. The former is characterized by the gravity acceleration g, and the latter—by the rigidity/elasticity parameter D. For pure gravity ($D = 0$) or purely flexural ($g = 0$) waves, the dispersion relation becomes of the power-type, $\omega \sim |\mathbf{k}|^{1/2}$ and $\omega \sim |\mathbf{k}|^{5/2}$, respectively. In such cases, there are no specific scales in the wave spectra, and as a result, the shapes of wave wakes in each of these cases do not depend on the source speed.

In contrast to that, the combined effect of gravity and rigidity removes the problem of degeneration: the minimal phase and group velocities provide characteristic scales. The corresponding dimensionless dispersion equation can be written as follows (see, e.g., Refs. [20,26]):

$$\sigma(\kappa_x, \kappa_y) = c_m M_p \kappa_x + \sqrt{|\boldsymbol{\kappa}|(1 + |\boldsymbol{\kappa}|^4)}, \quad |\boldsymbol{\kappa}|^2 \equiv \kappa^2 = \kappa_x^2 + \kappa_y^2, \tag{7}$$

where the dimensionless frequency and wave number $\sigma = \omega T$ and $\kappa_{x,y} = k_{x,y}L$, respectively, are scaled by the following quantities:

$$T = \frac{\bar{D}^{1/8}}{\sqrt{g}}; \quad L = \bar{D}^{1/4}; \quad \bar{D} = \frac{D}{\rho g}.$$

The dimensionless parameter $M_p = U/V_{\mathrm{pm}}$ plays a role of the *phase Mach number* as it represents the ratio of the current speed to the minimal phase speed of FGWs $V_{\mathrm{pm}} = c_m L/T$. This scaling is natural for the problem where the stationary shiplike wake can exist only when $M_p > 1$. The minimum of the dimensionless phase speed occurs at the wave number $\kappa_p = 3^{-1/4} \approx 0.76$ and equals to

$$c_m = \left.\frac{\sigma}{\kappa}\right|_{\kappa=\kappa_p} = 2\times 3^{-3/8} \approx 1.325. \tag{8}$$

Note, that the dimensionless frequency equals to unity at the minimum of phase velocity, $\sigma(\kappa_p) = 1$ (see Fig. 1).

A one more important parameter the *group Mach number*, $M_g = U/V_{\mathrm{gm}}$, can be introduced using the minimal group velocity, $V_{\mathrm{gm}} = c_M L/T$, where c_M is the minimal dimensionless group speed:

$$c_M = \left.\frac{d\sigma}{d\kappa}\right|_{\kappa=\kappa_g} = \left.\frac{1 + 5\kappa^4}{2\sqrt{\kappa + \kappa^5}}\right|_{\kappa=\kappa_g} \approx 0.878, \tag{9}$$

and $\kappa_g = (\sqrt{16/15} - 1)^{1/4} \approx 0.426$ is the positive root of the polynomial $15\kappa^8 + 30\kappa^4 - 1 = 0$. The group speed as the function of κ is shown in Fig. 1(b).

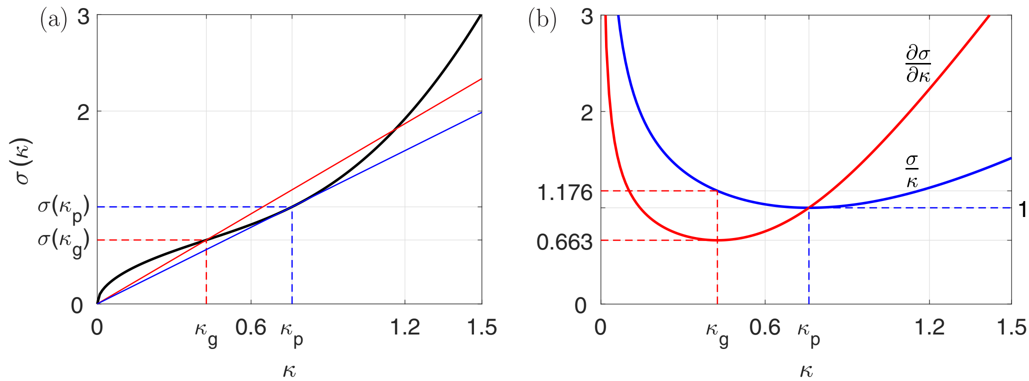

FIG. 1. (a) Dimensionless dispersion relations for flexural-gravity waves on deep water covered by a thin ice plate (black solid line) as per Eq. (7). The symbol κ_g shows the wave number where the group velocity has a minimum; the symbol κ_p shows the wave number where the phase velocity has a minimum. The blue solid line shows the dependence $\sigma = c_m\kappa \approx 1.325\kappa$, and the red solid line shows the dependence $\sigma = 1.176c_m\kappa \approx 1.558\kappa$. (b) Dimensionless phase (σ/κ) and group $(d\sigma/d\kappa)$ speeds as functions of dimensionless wave number κ.

The wave speed minima c_m and c_M, as well as the associated physical effects, are separated in the wave number space κ. As shown below, the corresponding Mach numbers M_p and M_g determine the geometry of wave patterns: demarkation of wake systems, occurrence of phase line cusps, characteristic angles, the counterparts of the classic Kelvin angle, etc. [2–5].

Figure 1(a) shows the intrinsic (in the absence of a current, $M_p = 0$) dimensionless dispersion relation (7) of FGWs by black solid line. As shown below, the point κ_p, where the minimum of the phase velocity occurs, conditionally separates two different intervals: (i) $0 < \kappa < \kappa_p$ where the gravity effects prevail and (ii) $\kappa > \kappa_p$ where the flexural effects prevail. The waves in these intervals can be treated as counterparts of purely gravity waves studied in Ref. [20] and purely capillary waves studied in Ref. [19]. Note that the magnitudes of the phase and group velocities coincide at $\kappa = \kappa_p$. Figure 1(b) shows the dimensionless phase and group velocities as functions of κ and the corresponding demarcation lines.

Following the dimensionless variables in the general analysis, one should keep in mind the characteristic values of key parameters for the real oceanic conditions. In contrast to the problem of gravity-capillary waves on a water surface, the counterpart of the capillarity parameter $\bar{D}$ can vary by more than two orders of magnitude (see Table I and references therein) depending on the ice plate thickness. As a result, the key physical parameter, the minimal phase speed V_{pm} can be easily surpassed by snowmobiles, not to mention airplanes during landing or take-off.

TABLE I. Parameters of floating ice sheets and characteristics of the flexural-gravity waves in the deep water.

Reference	$E\times10^{-9}$ N m^{-2}	h m	ν dim.-less	ρ kg m^{-3}	T s	L m	V_{pm} m s^{-1}	V_{gm} m s^{-1}	$\bar{D}\times10^4$ m^4
[33]	3.57	0.4	0.3	1000	0.83	6.75	10.78	7.15	0.213
[15] and this paper	5	1	0.3	1025	1.22	14.61	15.86	10.51	4.55
[7,11]	5	2.5	1/3	1000	1.72	29.04	22.36	14.82	74.66

III. GEOMETRY OF THE FLEXURAL-GRAVITY WAVE WAKE

A. Isophases of wave patterns and their asymptotes

Similar to the case of gravity-capillary waves, the minimum of the phase velocity determines the limit when stationary patterns on the ice plate can appear due to generation by a moving source. The condition of stationarity in the reference frame associated with the moving source, $\sigma = 0$, is

$$c_m M_p \kappa_x + \sqrt{\kappa + \kappa^5} = 0. \tag{10}$$

This equation follows from Eq. (7) and can be presented in the alternative form:

$$\cos\theta = \frac{\sqrt{\kappa + \kappa^5}}{\kappa\, c_m\, M_p}, \quad \text{where} \quad \kappa_x = -\kappa\cos\theta, \quad \kappa_y = \kappa\sin\theta. \tag{11}$$

The angle θ is counted from the negative direction of the x axis. The stationary harmonics with $\sigma = 0$ appear only when $M_p > 1$, i.e., when the current speed U exceeds the minimal phase velocity V_{pm} in the dimensional variables.

Then, to obtain a solution describing a wave wake, we need to find ray equations. These equations realize the principle of the minimal action (minimal phase, in wave problems) that generates the Hamilton function which is the frequency ω (or σ in dimensionless form) in our case (see, e.g., Ref. [34]). The stationarity condition (10) requires searching for a conditional extremum for the phase function. The corresponding Lagrangian multiplier t appears to be identical to the "physical" time in a general nonstationary problem (see Refs. [19,20] for discussion). In dimensionless coordinates

$$\xi = x/L; \quad \eta = y/L; \quad \tau = t/T, \tag{12}$$

which gives the solutions of the ray equation $\dot{\mathbf{x}} = \nabla_{\mathbf{k}}\omega$ for center of a wave packet:

$$\xi_0 = c_{g\xi}\tau = \left(-\frac{1 + 5\kappa^4}{2\sqrt{\kappa + \kappa^5}}\cos\theta + c_m M_p\right)\tau, \tag{13}$$

$$\eta_0 = c_{g\eta}\tau = \frac{1 + 5\kappa^4}{2\sqrt{\kappa + \kappa^5}}\sin\theta\,\tau. \tag{14}$$

These equations determine the geometry (or kinematics) of wave rays in the (ξ_0, η_0) plane. Let us define the phase functions $\varphi_0 = kx + ly = \kappa_\xi \xi_0 + \kappa_\eta \eta_0$ and write down them accounting for the condition of stationarity, $\sigma = 0$, in Eq. (7):

$$\varphi_0 = \frac{\tau}{2}\frac{\kappa(1 - 3\kappa^4)}{\sqrt{\kappa(1 + \kappa^4)}} = \frac{3\tau}{2}\frac{\sqrt{\kappa}\left(\kappa_p^4 - \kappa^4\right)}{\sqrt{1 + \kappa^4}}. \tag{15}$$

Then, the trajectories (13) and (14) can be presented in terms of phase φ_0:

$$\xi_0 = \frac{\varphi_0 \cos\theta}{3\kappa\left(\kappa_p^4 - \kappa^4\right)}\left(1 + 5\kappa^4 - 2\kappa c_m^2 M_p^2\right), \tag{16}$$

$$\eta_0 = \frac{\varphi_0 \sin\theta}{3\kappa\left(\kappa_p^4 - \kappa^4\right)}(1 + 5\kappa^4). \tag{17}$$

The isophase curve where $\varphi_0 = \text{const.}$ can be easily obtained then from Eqs. (16) and (17) accounting for the dependence of κ on θ as per Eq. (11).

The stationarity condition (10) or (11) determines the wave numbers κ in Eqs. (16) and (17) as functions of the angle θ that are the real roots of the fourth-degree polynomial. There are two such roots. The signs in the ray Eqs. (16) and (17) should be chosen to satisfy the radiation conditions or, in other words, the direction of energy propagation from the source of waves (see for detail [20] for the similar problem of gravity-capillary waves). The smaller root $\kappa_1 < \kappa_p$ can be attributed to negative dispersion gravity waves, whereas $\kappa_2 > \kappa_p$–to positive dispersion flexural waves. Accordingly, gravity waves whose energy transfers slower than the source moves form a wake behind the source [the sign minus in Eqs. (16) and (17)], whereas faster traveling flexural waves form a wake in front of the source [the sign plus in Eqs. (16) and (17)]. A separation line between two types of waves can be found from the condition of merging two real-valued roots in Eq. (10), i.e., when $\kappa_{1,2} = \kappa_p$. The formal limit $\kappa \to \kappa_p$ gives for wave directions

$$\lim_{\kappa \to \kappa_p} \cos\theta = \pm\frac{1}{M_p}, \tag{18}$$

or alternatively, for ray directions gives

$$\lim_{\kappa \to \kappa_p} \frac{\eta_0}{\xi_0} = \pm\frac{1}{\sqrt{M_p^2 - 1}}. \tag{19}$$

As follows from this formula, the separation lines asymptotically, approach the phase Mach cone $\xi_0 = \pm M_p \eta_0$ when $M_p \to \infty$.

B. Cusps of isophases: Group Mach number

The parametric trajectory dependences (16) and (17) on the wave number κ (or on the angle θ) lead to the cusp formations in the (ξ_0, η_0) plane. The cusps appear when the derivatives of both ξ and η with respect to κ (or with respect to θ) vanish simultaneously:

$$\xi'_\kappa = \eta'_\kappa = 0. \tag{20}$$

These equations lead to the 12-degree polynomial for κ_c in the cusp:

$$Z(\kappa_c) \equiv -15\kappa_c^{12} - 30M_p^2\kappa_c^9 + 111\kappa_c^8 - 60M_p^2\kappa_c^5 + 59\kappa_c^4 + 2M_p^2\kappa_c - 3 = 0. \tag{21}$$

The polynomial $Z(\kappa_c)$ is shown in Fig. 2(a) for several phase Mach numbers M_p. The equation similar to Eq. (21) was obtained for GCWs but in terms of the six-degree polynomial in Ref. [20].

The alternative representation of the conditions (20) provides an explicit dependence of the phase Mach number M_p on the wave number in the stationary points (20):

$$M_p^2 = \frac{1}{2c_m^2}\frac{-15\kappa_c^{12} + 111\kappa_c^8 + 59\kappa_c^4 - 3}{15\kappa_c^9 + 30\kappa_c^5 - \kappa_c}. \tag{22}$$

There are two vertical asymptotes that restrict the range of wave numbers for the cusps [see Fig. 2(b)]. As shown below, the lower boundary $\kappa_c = 0$ is associated with the cusps of gravity waves, and their locus is similar to the Kelvin cone. The upper boundary coincides with $\kappa_g \approx 0.426$ (see above) which corresponds to the minimum of group velocity M_g.

The dependence $M_p(\kappa_c)$ (22) has a minimum $M_p = M_p^{\text{cusp}} \approx 1.753$ at $\kappa_{\text{cusp}} \approx 0.332$. Two real roots of the polynomial $Z(\kappa_c)$ belong to different families of waves for $M_p > M_p^{\text{cusp}}$ [see Fig. 2(a)]. The smaller root $\kappa_c < \kappa_{\text{cusp}}$ corresponds to the cusp where the divergent and transverse waves meet similar to the classic deep water wave pattern [3,5,35]. The bigger root $\kappa_c > \kappa_{\text{cusp}}$ corresponds to the cusp where the divergent wave meets the so-called *fan wave* [22] associated with the minimum of group velocity and alternating wave dispersion at κ_g. This explains the introduction of the group Mach number M_g as the essential physical parameter of the problem.

Families of gravity and flexural waves can be easily discriminated in the dependences of the cusp wave vector direction θ_c and cusp polar angle $\beta_c = \arctan(\eta_c/\xi_c)$ on the dimensionless current speed: the phase M_p and group M_g Mach numbers as shown in Fig. 2(c) (cf. Fig. 2 in Ref. [19]). The wave cusp is characterized by the directions of the wave vector (angle θ_c) and wavefront (β_c). These directions are not orthogonal when $U \neq 0$. Lines denoted as “Kelvin cusps” in Fig. 2(c) correspond to the obliquely propagating negative dispersion gravity waves. These lines are weakly dependent on M_p and for large Mach numbers M_p and M_g they approach the classic Kelvin’s angles

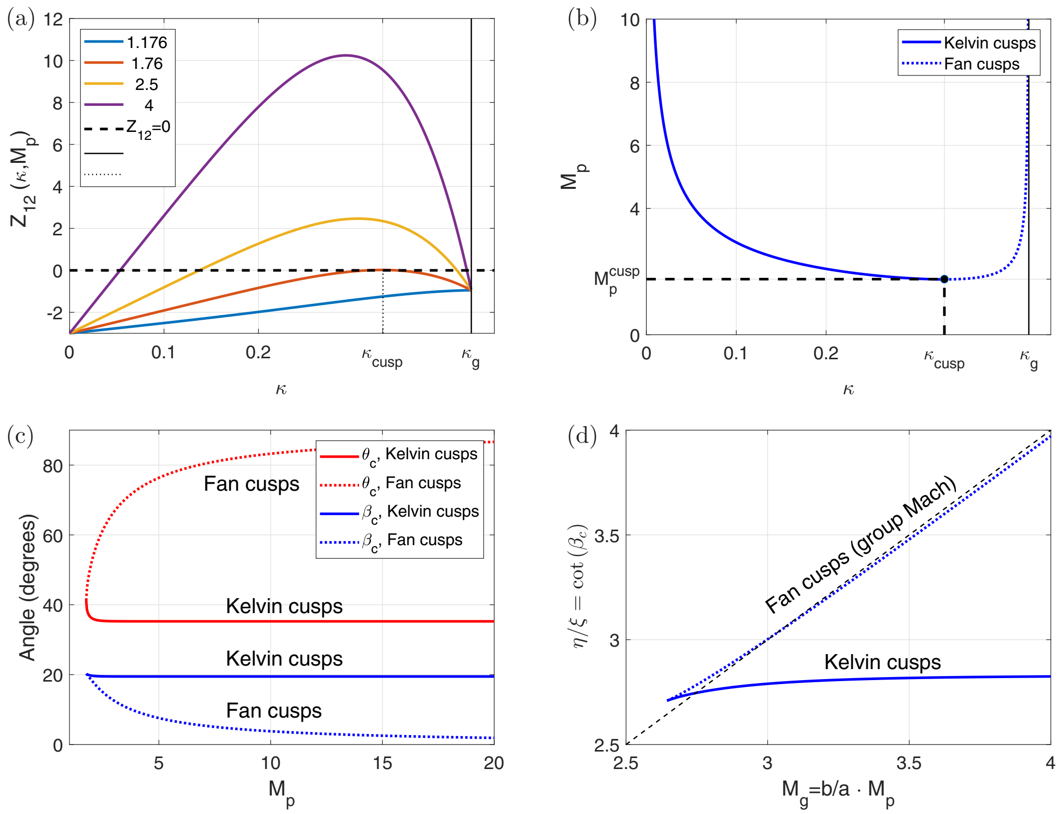

FIG. 2. (a) Polynomial $Z(\kappa)$ (21) for the different phase Mach number M_p (see the legend). (b) Dependence of M_p on the cusp wave numbers κ_c as per Eq. (19). (c) Angles of cusp lines in the coordinate (blue lines) and wave vector (red lines) spaces. (d) Dependence of the cusp loci $\eta_0/\xi_0 = \cot\beta_c$ on the group Mach number $M_g = c_m M_p/c_m$.

$\theta_{\mathrm{K1}} = \arcsin(1/3) \approx 19.47^\circ$ (Kelvin's cone half-opening) and $\theta_{\mathrm{K2}} = \arcsin(1/\sqrt{3}) \approx 35.26^\circ$ (wavefronts directions on the Kelvin's cone).

Dashed lines in Fig. 2(c) correspond to the negative dispersion branch of FGWs that form an additional family of isophase curves corresponding to so-called *fan waves* [22,23]. The dependence of the angle β_c in Fig. 2(c) is shown in Fig. 2(d) as the dependence of $\tan\beta_c = \eta_c/\xi_c$ on the group Mach number; this makes apparent simple asymptotics for the different wave families. Indeed, taking the limit $\kappa \to \kappa_g$, one can discover the asymptotic of the wave vector and wave isophases (wavefronts) (cf. similar results obtained for GCWs in Refs. [20,23,36]:

$$\lim_{\kappa\to\kappa_g} \cos\theta \approx \pm\frac{1.176}{M_p}; \quad \lim_{\kappa\to\kappa_g} \frac{\xi_c}{\eta_c} \approx \pm\frac{1.176(1.283M_p^2 - 1)}{\sqrt{M_p^2 - 1.383}}. \tag{23}$$

The corresponding cones in the wave vector and coordinate spaces appear when $M_p > 1.176$. For $M_p \gg 1$, the angle β_c is approaching β_g of the line with the minimal group velocity [see Eq. (11)]:

$$\lim_{\kappa\to\kappa_g} \frac{\xi_c}{\eta_c} = \lim_{\kappa\to\kappa_g} \cot\beta_g = \frac{c_M}{c_m} M_p \approx 1.509 M_p, \quad \text{where } \cos\beta_g = \frac{\sqrt{\kappa_g + \kappa_g^5}}{c_m\, M_p \kappa_g}. \tag{24}$$

This formula gives the *group Mach angle* β_g similar to that in the case of GCWs [19,22–26]. The dependence of β_g on $M_g\,(M_p)$ is not monotonic as shown in Fig. 3(a). It attains maximum at a

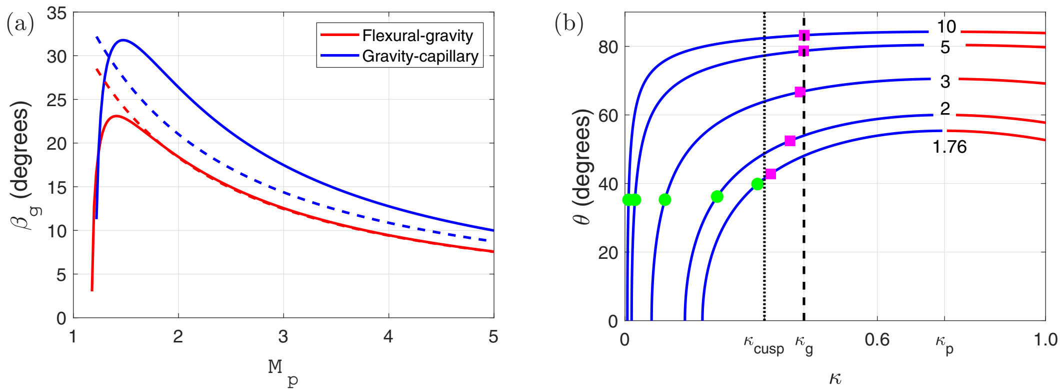

FIG. 3. (a) Dependence of the group Mach angle β_g on the phase Mach number M_p for FGWs and, for the comparison, for GCWs (see the legend). Dashed curves show the asymptotic dependences of the corresponding curves for big M_p. (b) Dependencies of wave directions on the wave number for different phase Mach numbers (shown by numbers). Symbols show cusp points: green dots pertain to Kelvin's cusps, magenta squares—to fan wave cusps.

relatively low value of $M_p \approx 1.417$ and then, gradually approaches the asymptote (24). The similar dependence for GCWs has a bigger maximum at slightly bigger M_p. It can be noted a remarkably fast convergence of the FGW dependence onto the asymptote (24) as compared to the GCWs counterpart [19].

Figure 3(b) shows the dependence of wave vector direction θ_c on the wave number for different phase Mach numbers M_p. The classic case of deep water gravity waves looks degenerate due to the scale-invariance, i.e., the absence of a characteristic physical scale. As aforementioned, the latter makes the Kelvin angle independent of the source speed. The flexural force introduces a characteristic scale that establishes a balance between the gravity and flexural effects. The wave numbers and characteristic angles (for example, wave directions in the cusp points) become tightly linked when the balance is reached for the characteristic scale and dimensionless parameters; Fig. 3(b) illustrates this link.

The analysis presented above can be summarized in terms of the increasing value of the phase Mach number M_p:

(1) At $M_p = 1$ the Mach cone with the angle of half-opening of 90° arises being associated with the minimal phase velocity [see blue solid line in Fig. 1(a)];

(2) At $M_p \approx 1.176$ the Mach cone associated with the minimal group velocity appears [see red solid line in Fig. 1(a)]. In the range, $1 \leqslant M_P \leqslant 1.176$ waves of positive dispersion are generated [the dispersion curve is concave up as shown in Fig. 1(a) by the black solid line]. Then, at $M_p = 1.176$, "a soft bifurcation" occurs because waves of negative dispresion with $\kappa < \kappa_g$ appear at $M_p > 1.176$. However, wave patterns in the wake remain smooth with no cusps;

(3) At $M_p \approx 1.417$ the group cone opening with the angle β_g is maximal;

(4) At $M_p \approx 1.754$ "a stiff bifurcation" occurs when a pair of cusps appears on the isophase curves;

(5) At $M_p > 1.754$ formation of cusps and different wave systems occur, namely, divergent and transverse waves of negative dispersion (similar to those in purely gravity ship waves) and a new system of the so-called fan waves in between the phase and group Mach cones.

All these bifurcations are illustrated by Fig. 4. The emergence of cusps has an important influence on wave amplitudes. The overlapping of isophases means that more than one wave ray arrives at the point. Thus, the resulting solution is a superposition of two or even three particular rays arriving at the same point.

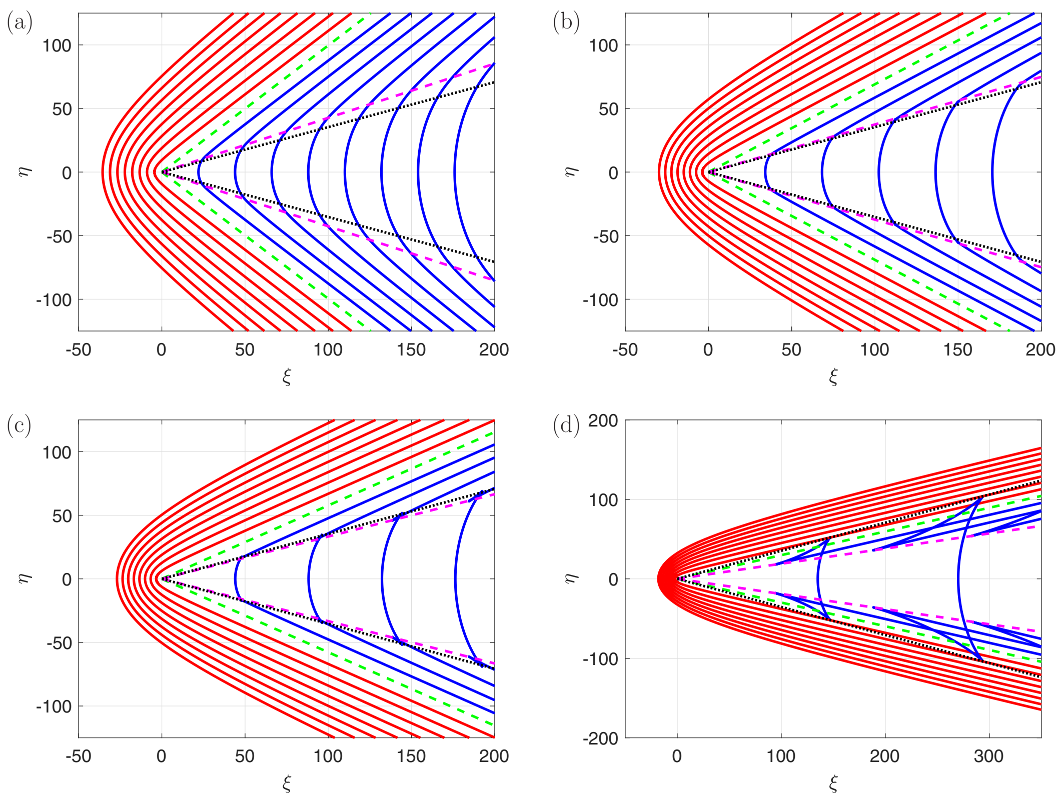

FIG. 4. Isophases of stationary wave patterns at different dimensionless speeds, i.e., phase Mach numbers M_p. Red curves show the elastic wave family while the gravity wave family is shown by blue lines. Dashed green lines depict the phase Mach cones which serve as the demarcation lines between the elastic and gravity wave families. Dashed magenta lines show the group Mach cones; dotted black lines represent the classic Kelvin cone $\beta_K = \arctan(1/\sqrt{8})$. In frame (a) $M_p \approx 1.417$, where the maximal opening of the group Mach cone occurs; in frame (b) $M_p \approx 1.76$, which corresponds to the minimal speed when the cusps appear; in frame (c) $M_p = 2$; in frame (d) $M_p = 4$, where fan wavefronts become parallel to the demarcating green dashed line.

C. Isophase patterns

To illuminate solutions derived in the previous subsection, we plot the FGW isophase patterns in Fig. 4 for different phase Mach numbers M_p. The maximal opening of the group cone (see magenta dashed line) in Fig. 4(a) is slightly bigger than the classic Kelvin angle $\beta_K = \arctan(1/\sqrt{8})$ shown by black dotted line. The phase Mach cone shown by the green dashed line demarcates isophases of families of gravity (blue lines) and flexural (red lines) waves at big distances from a source. The cusps appear at $M_p \approx 1.76$ [see Fig. 4(b)] when the group Mach cone is slightly wider than the Kelvin cone. When the phase Mach number approaches $M_p = 2$, the group Mach angle becomes smaller than the Kelvin angle $\beta_K = \arctan(1/\sqrt{8})$ [see Fig. 4(c)].

Two families of cusps lie on two different lines. The outer family approaches the Kelvin angle and is associated with the transversal and divergent systems of waves well-known from the classic patterns of pure gravity waves [2–5]. The inner cusp locus converges to the group Mach angle and becomes a starting point of a new family of fan waves, introduced in Ref. [22] for GCWs. In the range of angles between the outer cusp locus (the counterpart of the Kelvin cone) and inner locus (fan waves) given by the group Mach cone, two different rays arrive at each point (ξ, η). Thus, the superposition of two wave systems appears.

At $M_p \approx 3$ the locus of the inner cusps (close to the classic Kelvin line) matches the phase Mach cone and enters the domain of the family of flexural waves at higher values of M_p. Each point in the sector between the Kelvin and phase Mach cones contains three wave rays (three characteristics). In addition to the well-known rays of transversal and divergent waves typical for ship waves, the ray of flexural waves of positive dispersion appears [see Fig. 4(d)]. At high speeds [for example, at $M_p = 4$ as in Fig. 4(d)], the isophases of fan waves become parallel to the demarcating line of the phase Mach cone (shown by green dashed line), and the inner cusps approach their locus at the group Mach cone (shown by magenta dashed line).

Thus, we have described in detail the kinematics of wave patterns in the wake as a function of the phase Mach number M_p. In the result, we obtained a fairly rich picture by varying only one dimensionless parameter and discovered two specific features associated with the phase and group speeds. The number of rearrangements in the wake pattern occurs when the parameter M_p increases. The group cone appears at $M_p \approx 1.176$ (see Fig. 1(b)), reaches its maximum opening at $M_p \approx 1.417$, and then tapers off monotonically. At $M_p \approx 1.76$ the caustics appear and the corresponding domain between the Kelvin and group Mach cones acquires a new feature: each coordinate point in this domain contains two rays of the gravity wave family. When the phase Mach cone shrinks narrower than the Kelvin one, the two-ray domain becomes limited by two Mach cones: the phase and group. The domain between the Kelvin cone and the phase Mach cone appears to become more complicated: each coordinate point (ξ, η) contains three different characteristics. In addition to two rays of the gravity wave family, one more ray of flexural waves emerges when caustics enter the domain of flexural waves. Below we present the dynamics of a wave wake and see that one more dimensionless parameter arises that describes the wave amplitude distribution in the wake.

IV. REFERENCE SOLUTION FOR THE AMPLITUDE IN THE SHIP WAKE OF FLEXURAL-GRAVITY WAVES

A. Reference solution parameterized by the wave number κ and angle θ

Expressions for the wave amplitude within the wake of a finite-size moving source can be obtained following the works [18–20] in the form of parametric dependences of the solution on the wave number κ (or the angle θ) and the phase φ_0 [see Eqs. (15)–(17)]. The transformation of a solution to the coordinates ξ, η can lead to multivalued dependences which correspond to the arrival at a given point of two or more rays with different phases φ_0. Such events can be easily predicted through the analysis of isophase patterns as described in Sec. III.

The wave amplitude in the linear approximation represents a superposition of different wave fields. The contribution of pure gravity waves in the total wave field can be easily separated because of their scale invariance mentioned above. The isophase lines do not depend on the wave number but on the angle θ only (see Ref. [20] for details). In general, both κ and θ enter the parametric dependences that make the problem more intricate mathematically. In this study, we present the analysis of the simplest case when cusps are absent and each point (ξ, η) is characterized by the only wave ray. Even in this case of a relatively low speed of a source (or a corresponding flow), when $M_p < 1.76$, a variety of interesting physical effects already exist.

Exploiting the Reference Solution Method described in Refs. [18–20] in application to gravity-capillary waves, we consider the dynamics of a linear Gaussian packet:

$$F(\xi, \eta, \tau) = \frac{1}{\sqrt{\Lambda}} \exp\left[-\frac{\Phi^2(\tilde{\xi}, \tilde{\eta}, \tau)}{2\Lambda^2}\right] \cos(\varphi_0 + \varphi_1), \tag{25}$$

where $\tilde{\xi} = \Delta\kappa_\xi(\xi - \xi_0)$, $\tilde{\eta} = \Delta\kappa_\eta(\eta - \eta_0)$, $\Delta\kappa_\xi$, $\Delta\kappa_\eta$ are spectral widths of the pulse, function $F(\tilde{\xi}, \tilde{\eta}, \tau)$ describes the dimensionless deflection of the ice plate, the phase function φ_0 defined in Eq. (15) characterizes the distance from the source in terms of number of waves, φ_1 will be determined below, $\Phi^2(\xi, \eta, \tau)$ is the positively defined quadratic form:

$$\Phi^2(\tilde{\xi}, \tilde{\eta}, \tau) = \tilde{\xi}^2\left[1 + \tau^2\left(\mu_{\xi\eta}^2 + \mu_\xi^2\right)\right] + \tilde{\eta}^2\left[1 + \tau^2\left(\mu_{\eta\xi}^2 + \mu_\eta^2\right)\right] - 2\tilde{\xi}\tilde{\eta}\tau^2\mu_{\xi\eta}(\mu_\xi + \mu_\eta), \tag{26}$$

and $\Lambda(\tau)$ is the instant half-width of the Gaussian packet [18]:

$$\Lambda^2(\tau) = \Lambda_0^2\left[1 + \tau^2\left(2\mu_{\xi\eta}^2 + \mu_\xi^2 + \mu_\eta^2\right) + \tau^4\left(\mu_{\xi\eta}^2 - \mu_\xi\mu_\eta\right)^2\right]. \tag{27}$$

Here Λ_0 is the initial dimensionless width of the Gaussian packet (it plays a role of the Bond number for FGWs, $\Lambda_0 = d/L = d(\rho g/D)^{1/4}$, where d is the dimensional initial longitudinal size of the packet, similar to the Bond number for GCWs [23]); the other quantities in this formula are

$$\mu_\xi = (\Delta_\xi)^2 \frac{d^2\sigma}{d\kappa_\xi^2}, \quad \mu_\eta = (\Delta_\eta)^2 \frac{d^2\sigma}{d\kappa_\eta^2}, \quad \mu_{\xi\eta} = \Delta_\xi\Delta_\eta \frac{d^2\sigma}{d\kappa_\xi d\kappa_\eta}. \tag{28}$$

Further, we assume that the following dimensionless parameters are small:

$$\Delta_\xi = \frac{\Delta\kappa_\xi}{\Lambda_0\kappa} \ll 1; \quad \Delta_\eta = \frac{\Delta\kappa_\eta}{\Lambda_0\kappa} \ll 1. \tag{29}$$

These parameters characterise a wave spectrum; together with the phase or group Mach numbers they play an important role in the description of a wave field. The defined parameters can be combined into two groups. One of them is the product $\Delta_\xi\Delta_\eta \equiv E$ which is proportional to the pulse energy for the Gaussian wave packet (25). Another parameter, $\alpha = \Delta_\eta/\Delta_\xi$, is the length-to-beam ratio of a two-dimensional Gaussian pulse. In our study, these parameters play an essential role therefore, we will focus on their influence on the wave field. As well known, the energy parameter E is absent in the SPA; therefore, an attempt to describe the dynamics of finite-size wave packets within the SPA faces serious problems. Meanwhile, as shown below, such a description based on RSA is simple and transparent (note that a similar description can be achieved with the help of the saddle point method [37]). However, some attempts to describe the dynamics of finite-size pulses in water waves have been undertaken based on the SPA too (see, for example, Ref. [38]). The outcome is qualitatively close to what can be obtained with the help of RSA but with more difficulties and less physical transparency. Moreover, the generalization of this result to FGWs is not straightforward.

Note that Eq. (27) can be rewritten in the following form:

$$\Lambda^2 = \Lambda_0^2[(1 - A)^2 + B^2], \tag{30}$$

where

$$A = \tau^2\left(\mu_{\xi\eta}^2 - \mu_\xi\mu_\eta\right); \quad B = \tau(\mu_\xi + \mu_\eta). \tag{31}$$

The alternative form of Λ (30) separates the effects of dispersion and spatial divergence. Generally, when $A \neq 0$, we have the normal amplitude decay: $|F| \sim \tau^{-1} \sim r^{-1}$. One can treat this decay as the result of simultaneous effects of the cylindrical divergence ($\sim r^{-1/2}$) and dispersion ($\sim r^{-1/2}$). If A vanishes ($\mu_{\xi\eta}^2 = \mu_\xi\mu_\eta$), then the term B becomes dominant in Eq. (30). In this case the amplitude of the wave field decays much slower, $|F| \sim \tau^{-1/2}$ under the influence of dispersion only, whereas a geometric divergence vanishes within certain directions—see below.

Equations (25)–(29) are quite general and are applicable to any kind of waves. Specifically for the FGW they can be rewritten as the explicit dependences on the wave number κ (or angle θ) and phase function φ_0 (cf. Eqs. (41)–(43) in Ref. [19]):

$$A = \frac{5}{6}\frac{\left(\kappa^4 - \kappa_g^4\right)}{\left(\kappa^4 - \kappa_p^4\right)^2}\frac{(1 + 5\kappa^4)\left(\kappa^4 + \kappa_g^4 + 2\right)}{(\kappa^4 + 1)}\varphi_0^2E^2, \tag{32}$$

$$B = \frac{\varphi_0 E}{3\left(\kappa^4 - \kappa_p^4\right)}\left[\frac{1}{\alpha}(K\sin^2\theta + R\cos^2\theta) + \alpha(K\cos^2\theta + R\sin^2\theta)\right], \tag{33}$$

$$K = 1 + 5\kappa^4, \quad R = \frac{15\left(\kappa^4 - \kappa_g^4\right)\left(\kappa^4 + \kappa_g^4 + 2\right)}{2(1 + \kappa^4)}. \tag{34}$$

The wave number κ labels rays along the wave field. The term A vanishes along the ray $\kappa = \kappa_g$, i.e., at the group Mach cone that, as said above, leads to the anomalously slow amplitude decay along such a ray. Therefore, one can clearly see on the (ξ, η) plane a group cone where the wave amplitude attains a maximum and slowly decays along the ray. A selection and visualisation of the group ray in the wave wake is the advantage of the RSA.

On the phase Mach cone, $\kappa = \kappa_p$, the expressions for A and B in Eqs. (32) and (33) become uncertain because the phase φ_0 vanishes at the point $\kappa = \kappa_p$ [see Eq. (15)], together with the denominators of A, B. The vanishing of the phase φ_0 on the phase Mach cone determines the ray $\kappa = \kappa_p$ which separates the gravity and flexural families of waves described by different signs in expressions (15).

The phase function φ_0 (15) appears in the argument of cosine in Eq. (25) as the phase of the carrier wave [18] therefore, it can be regarded as the kinematic characteristics. The additional phase shift φ_1 is associated with the finite size of the Gaussian reference pulse and can be written as (see its derivation in the Appendix, see also Refs. [18,19]):

$$\varphi_1 = \frac{1}{2} \arctan \frac{B}{1 - A}. \tag{35}$$

This phase depends on wave parameters in contrast to its counterpart in the method of stationary phase where this phase shift is fixed $\pm\pi/4$. Note that a similar formula was obtained by Kelvin [35] in a one-dimensional case. Thus, the reference solutions mimic essential features of the stationary phase method adding new peculiarities.

B. Spatial structure of the reference solutions

Equations (32)–(34) provide all necessary elements for the calculation of amplitudes, phases, and the resultant wave patterns generated by the Gaussian source (25) for given ray markers which are either the wave numbers κ or angles θ. The further mapping of the dependences into the coordinate space is not so straightforward: the rays of different κ (or θ) arrive at the same point of the coordinate space. There is no problem with the simple summation of amplitudes in the corresponding parts of the coordinate plane. The problem is only associated with the occurrence of cusps. The volume of a wave packet D remains a single-valued function of spatial coordinates in two cases:

(1) When the phase Mach number is relatively small, $M_p < 1.754$, in all coordinate plane;

(2) In the interior of the group Mach cone $\cot \beta = M_g$ at any values of the phase Mach number M_p.

The pair of cusps at $M_p > 1.754$ for the gravity branch of waves outlines the cone where a pair of rays determines the wave field in each coordinate point. The inner bound of the cone, fan cusps loci, converges to the group Mach line [see Fig. 2(d)]. In contrast, the outer bound represents the Kelvin family of cusps which rapidly approaches the classic Kelvin angle $\Theta_K = \arctan(1/\sqrt{8})$. As follows from Eq. (19), at the phase Mach number $M_p \approx 3$, the phase Mach angle $\arctan(\eta_0/\xi_0) = (M_p^2 - 1)^{-1/2}$ matches the Kelvin cusp locus and the isophases of flexural family of the wave wake enter the domain of gravity waves [see blue isophases in Fig. 4(d)]. In the corresponding domain within the Kelvin and phase Mach angles each coordinate point contains three rays: two characteristics of the gravity family with sign plus for the phase φ_0 in Eq. (15) and one for the flexural family with the sign minus of φ_0.

C. Amplitude and phase patterns of FGW at small Mach numbers

In this section, we present illustrations for wave patterns at relatively low source speeds when $M_p < 1.754$. Then, cusps are absent, and the equation for a wave amplitude contains a single term. The limitation of low source speeds is of practical interest. As seen from Table I, minimal phase speeds of FGW are quite high and the most of on-ice activity occurs at Mach numbers below the critical value $M_p \approx 1.76$. The essential physical effects can be found under such a limitation. In the meantime, in general, the problem of the construction of wave wakes at high speeds is rather technical than scientific.

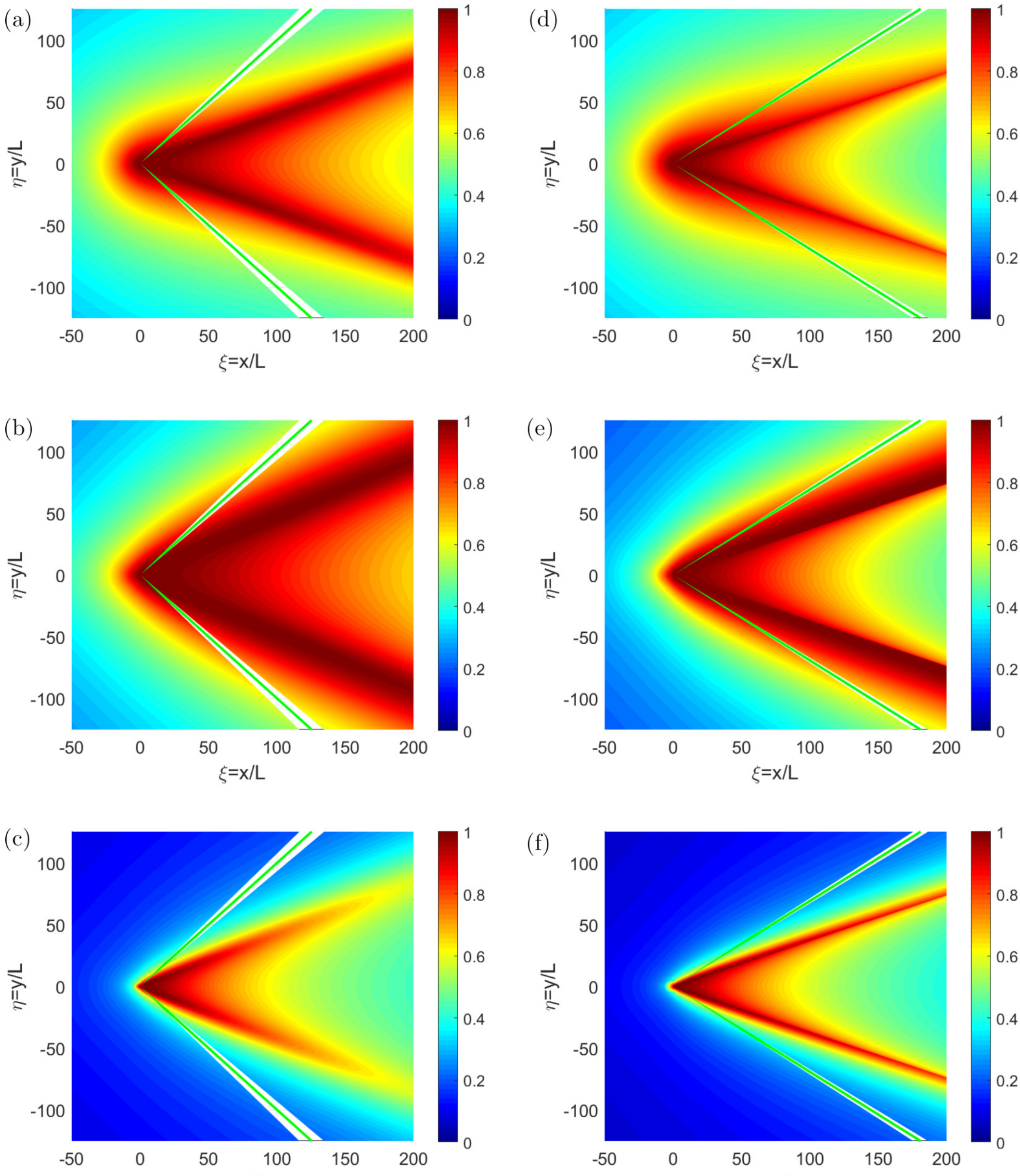

FIG. 5. Amplitude wave patterns generated by sources of different shapes moving at two different speeds. Frames (a)–(c) $M_p = 1.417$; frames (d)–(f) $M_p = 1.75$. The upper row pertains to a wide source, $\alpha = \Delta_y/\Delta_x = 1/3$; middle row—to a circular source, $\alpha = \Delta_y/\Delta_x = 1$; lower row—to an elongated source, $\alpha = \Delta y/\Delta_x = 3$.

In Fig. 5 we show the amplitude factor $\Lambda^{-1/2}$ that reflects long-scale wave wake variability for different source speeds and different aspect ratios α. Our formulas allow us to construct wave wake patterns from the far-field zone up to the near-field zone. Further, to focus on the effect of the source shape, we fix the dimensionless energy parameter $E = 2.5\times10^{-3}$ and consider two values of the phase Mach number M_p. The case $M_p = 1.417$ corresponds to the maximal opening of the group Mach cone. The second case $M_p = 1.75$ is very close to the threshold of appearance of wave cusps

($M_p \approx 1.754$) when the simple transformation from the wave number space to the coordinate space breaks. The left frames of Fig. 5 pertain to the lower Mach number $M_p = 1.417$, and the right frames—to a bit higher number $M_p = 1.75$. The upper row shows the patterns generated by a wide source with $\alpha = 1/3$, middle row—by a circular source with $\alpha = 1$, and the bottom row—by the elongated sources with $\alpha = 3$. The pronounced effect of source shape is illustrated by the up-stream perturbations shown in Figs. 5(a) and 5(d) for the wide source in comparison with Figs. 5(c) and 5(f) for the narrow source. The circular source generates notable perturbations in both up- and down-stream directions as shown in Figs. 5(b) and 5(e). The elongated source $\alpha = 3$ emphasizes the phase Mach cone while perturbations rapidly decay in other directions.

In Fig. 6 the wave surface elevations and the phase correction φ_1 are shown for the subcritical Mach number $M_p = 1.75$. The pronounced effect of the source shape on φ_1 is seen in the right column. A circular source represents a sort of reference case: the abrupt change of φ_1 from zero in the group cone interior to $\pi/4$ occurs then φ_1 is slowly varies to higher values. It can be noted that in this case, the group Mach angle is very close to the line where cusps occur, i.e., to the Kelvin angle [see Fig. 4(b)]. The relation with the stationary phase method where the phase steplike shift $\pi/4$ appears at the caustic looks quite natural. In the meantime, the patterns produced by wide and narrow sources shown in Figs. 6(d) and 6(f), respectively, look more sophisticated.

The left column of Fig. 6 shows the resultant wave patterns that account for both the amplitude and phase effects; they are complementary to those shown in Figs. 5 and 6(d)–6(f).

V. DISCUSSION AND CONCLUSIONS

In this paper, we have studied a wave wake produced by a finite-size source uniformly moving on an ice plate overlying deep water. As mentioned in the Introduction, such a problem is topical and of practical interest due to the exploration of polar zones, as well as, due to the construction of very large floating platforms and solar panels. In all such cases, an important role plays the elasticity of a plate covering a sea or an ocean; the elasticity together with the gravity effect gives rise to flexural-gravity waves.

We have described the kinematic characteristics of flexural-gravity waves and determined various directions where wave phases remain constant and form patterns on the plane. Pattern configurations depend on the speed of the source. It is shown that specific cusps emerge in the patterns when the source speed exceeds threshold values. When the source speed exceeds the first threshold value V_1, the emerging cusps are similar to those known for gravity waves in deep water when two different waves, transversal and longitudinal (divergent), start to overlap. When the source speed exceeds the second threshold value $V_2 > V_1$, the cusps are formed by the overlapping of three wave types, transversal, longitudinal, and fan. Such a situation resembles a wave wake of gravity-capillary waves in deep water. This is illustrated by Fig. 4. Our results generalize the classic Kelvin's results who found a universal ship wake for gravity waves in deep water. We have demonstrated that due to the presence of the characteristic spatiotemporal scale in the spectrum of FGWs, the wake is not self-similar in contrast to pure gravity waves but essentially depends on the speed of a source.

To describe wave amplitudes, we use the RSA. This approach allows one to obtain analytical results of phase and amplitude distributions of ship-type wakes. The results obtained provide the same general features of wave phase distribution that can be captured by other asymptotic approaches, for example, by the best-known and widely used method of stationary phase. Moreover, the RSA allows one to quantify wave dynamics of the finite-size source and describe wave wake not only asymptotically in the far-field zone but also in the intermediate wave zone that cannot be captured by the SPA. Specific effects of the length-to-beam ratio of amplitude and phase features in this zone are presented here for the first time.

The analytical results relate the kinematic and dynamic effects with the minima of phase and group velocities where the character of FGWs dispersion changes from the negative one for long waves to the positive one for short waves. The problem scaling in the different ranges of wavelengths allows one to present results universally. It is worthwhile to emphasise that the nonmonotonic

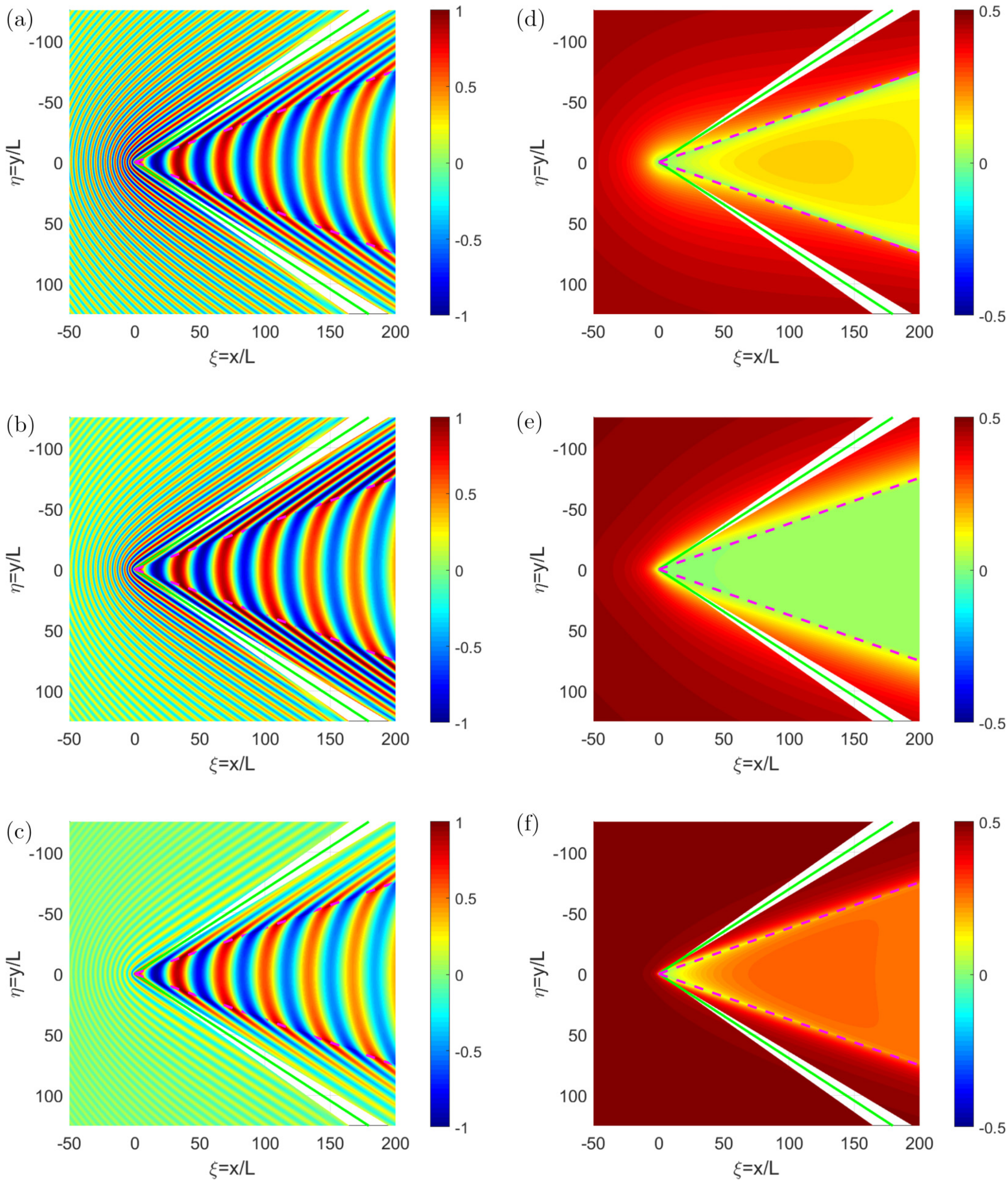

FIG. 6. Left column: surface elevations together with the wave phases generated by sources of different shapes at $M_p = 1.75$. Frames (a)–(c): top—a wide source, $\Delta_y/\Delta_x = 3$; middle—a circular source $\Delta_y/\Delta_x = 1$; bottom—a narrow source $\Delta y/\Delta x = 1/3$. Right column shows the phase correction φ_1.

dependence of wave speeds (both the phase and group) in the considered problem provides a natural scaling that separates gravity and flexural waves. Formally, the whole problem can be investigated using only one such scale; however, it is convenient to operate with two different scales related to the minima either of the phase or group speed using either the phase Mach number M_p or the group Mach number M_g, respectively, depending on the considered effects. In particular, the kinematic effects in the wave wake can be naturally described in terms of M_p, whereas the dynamic effects can be naturally described in terms of M_g [note that according to Eqs. (8) and (9), the ratio of $c_m/c_M \approx 1.51$]. As shown in the paper, bifurcations occurring in the wave wake patterns when the corresponding Mach numbers increase can be easily followed within the ray equations. We have illustrated them with figures and have demonstrated that the bifurcations are directly linked with the overlapping of different kinds of waves, transversal, longitudinal (divergent), and fan.

We have shown that along the group Mach cone, the wave amplitude decays anomalously slow, $\sim\varphi^{-1/2}$. This is related to the existence of the group speed minimum. The existence of the phase speed minimum provides separation to different families of waves at relatively low speeds ($M_p \lesssim 3$), whereas at greater speeds, the domains of gravity and flexural waves overlap. This leads to complications in the mathematical description of the problem when three different wave rays arrive at the same coordinate point.

The application of the RSA allows us to study the effect of a source shape on the structure of wave wakes. The source-shape effect has been illustrated by the amplitude distributions shown in Figs. 5 and 6. In the conclusion, we mention a few more advantages of the RSA compared to SFA. The RSA describes wave phases adequately in the entire plane, whereas within the SPA, the phases break near caustics (cusps). The RSA predicts a continuous transition between different wave zones where one, two, or even three different rays overlap.

A further development of results obtained and more advanced analysis of a wake produced by a finite-size source by the RSA can be made numerically which we plan to do in the near future. Some other aspects of wave motion generated by various sources on an ice sheet can be also studied by means of the RSA; in particular, ice compression, shear flows, finite ocean depth, water stratification [16,39], nonstationary motion [40], etc.

Notes added. Recently, we become aware about a few more publications relevant to our work. In the papers [41,42], the authors studied far fields FGWs in the infinitely deep ocean covered by an ice plate generated by the uniform flow around a localized source situated at some depth. In the linear approximation the authors presented solutions through the Fourier integrals and constructed their asymptotics using the stationary-phase method. The integrals were calculated numerically and compared against the asymptotic results for the particular sets of physical parameters. It was shown that main effect on the generated wave patterns is due to the ice cover thickness and the flow velocity. The results obtained in these papers reproduce the results obtained by Davys *et al.* in 1995 [7].

In Ref. [43] the authors determined critical speeds at which the nature of the wave disturbance drastically changes when a load source moves on an ice plate. The angular zones in which FGWs propagate as well as wave amplitudes are determined for the particular values of water depth, source speed, thickness of the ice plate, and compression and tension forces exerting on it. Two critical source speeds V_1 and V_2 are determined which show that to avoid ice destruction, the vehicle speed must be beyond the interval (V_1, V_2). However, to destroy effectively an ice plate by a moving source (for example, by an air cushion vehicle), its speed must equal to one of the critical speeds V_1 and V_2. In Ref. [44], the same authors studied FGW generation under the action of a moving and oscillating pressure disturbance $p = p_0 f(x - Vt, y)e^{i\omega t}$. The values of critical speeds at which the nature of the wave disturbance changes were determined, both in front of the disturbance source and behind it. The dependence of critical velocities on the frequency of source oscillations ω was studied, and six values of critical speeds were obtained. It was shown that from one to seven systems of waves on the ice plate can be formed depending on the source speed. The angular zones in which these waves are formed were determined. The influence of compression and tension forces on the values of critical speeds and angular zones in which waves can propagate were studied. A similar problem was studied in Ref. [45], but it was assumed that a pulsating point source was located in a uniform water flow at some depth in the fluid of a finite depth.

In the recent paper of Ref. [46], Tkacheva studied wave patterns on an ice plate arising under the action of a moving source of a rectangular shape in the presence of a shear flow with a constant vertical gradient in the fluid beneath the plate. The problem was studied in the dimensionless variables taking into account a uniform ice plate compression and finite fluid depth. The motion of the load source could be at an arbitrary angle to the direction of the fluid flow. The critical source speeds and the deflection of ice cover were found numerically for the different shear flow gradients, angles between the source and shear flow velocities, and compression ratio of the ice plate. The wave patterns on the ice plate by a moving source are illustrated numerically for different parameters.

In almost all papers cited above (except Ref. [46]), the authors considered the problem of FGWs generation for the particular sets of dimensional parameters which are quite realistic but do not embrace all possible cases; the results obtained were presented in forms of tables and plots. In our paper, we presented the results in the universal dimensionless variables for infinitely deep ocean without compression or tension forces exerting on a moving source. This allows one to determine a minimal number of governing parameters and manipulate with all other dimensional parameters.

ACKNOWLEDGMENTS

S.B.'s research was supported by RSF Grant No. 19-72-30028 "Turbulence and coherent structures in the integrable and nonintegrable systems." V.G. acknowledges the financial support of the Ministry of Science and Higher Education of the Russian Federation through Grant No. FMWE-2024-0017. Y.S. acknowledges the financial support of the Ministry of Science and Higher Education of the Russian Federation through Grant No. FSWE-2023-0004. The authors are grateful to I. V. Sturova who provided us with additional references.

The authors report no conflict of interest.

APPENDIX: REFERENCE SOLUTION METHOD

Following the ideas presented in Ref. [18], consider a linear solution in the dimensional form for the vertical deflection w of an ice plate from the undisturbed position through the Fourier integral (the resultant formulas derived in this Appendix are presented in Sec. IV A in the dimensionless form):

$$w(\mathbf{x}, t) = \mathrm{Re}\left(\frac{1}{2\pi} \int_{-\infty}^{+\infty} F(\mathbf{k}) e^{i[\mathbf{k}\mathbf{x} - \omega(\mathbf{k})t]}\right) d\mathbf{k}. \tag{A1}$$

Here symbol Re stands for the real part of the corresponding expression, $F(\mathbf{k})$ is the Fourier image of the function $w(\mathbf{x}, 0)$ at initial time moment $t = 0$.

Consider the initial disturbance $w(x, y, 0) \equiv f(x, y)$ in the form of a Gaussian wave packet:

$$f(x, y) = \mathrm{Re}\left(\frac{1}{\Delta x \Delta y} \exp\left[-\frac{x^2}{2(\Delta x)^2} - \frac{y^2}{2(\Delta y)^2}\right] e^{i(k_0 x + l_0 y)}\right). \tag{A2}$$

Note, that in the limit $\Delta x \to 0,\ \Delta y \to 0$ Eq. (A2) reduces to

$$\lim_{\Delta x \to 0,\ \Delta y \to 0} f(x, y) = \tfrac{1}{2} \delta(x - x_0) \delta(y - y_0) \cos(k_0 x + l_0 y). \tag{A3}$$

This property will be used below to construct solutions for a wave of a source with a finite Fourier spectrum. The Fourier transform (A2) of the initial function (A2) is a normalized Gaussian pulse:

$$F(k, l) = \exp\left[-\frac{\kappa_x^2}{2(\Delta k)^2} - \frac{\kappa_y^2}{2(\Delta l)^2}\right], \tag{A4}$$

where $\kappa_x = k - k_0,\ \kappa_y = l - l_0$ and

$$\Delta k = 1/\Delta x; \quad \Delta l = 1/\Delta y. \tag{A5}$$

Assuming the pulse (A4) is narrow-banded, i.e., $\Delta k/k_0 \ll 1,\ \Delta l/l_0 \ll 1$, we approximate the dispersion relation $\omega(\mathbf{k})$ in Eq. (A1) by its Taylor series in the vicinity of the wave packet carrier wave vector $\mathbf{k_0}$:

$$\omega(\mathbf{k}) = \omega_0 + \omega_k' \mid_{\mathbf{k}} = \mathbf{k_0} \cdot \kappa_x + \omega_l' \mid_{\mathbf{k}} = \mathbf{k_0} \cdot \kappa_y + \tfrac{1}{2}(\mu_x + \mu_y + 2\mu_{xy}) + O(|\kappa|^{\mathbf{3}}), \tag{A6}$$

where the symbol prime stands for a derivative with respect to the corresponding variable shown as the index, and

$$\mu_x = \omega''_{kk} \mid_{\mathbf{k}} = \mathbf{k}_0 \cdot (\Delta k)^2; \quad \mu_y = \omega''_{ll} \mid_{\mathbf{k}} = \mathbf{k}_0 \cdot (\Delta l)^2; \quad \mu_{xy} = \omega''_{kl} \mid_{\mathbf{k}=\mathbf{k}_0} \cdot \Delta k \Delta l. \tag{A7}$$

After that, the resulting approximation of the integral (A1) takes the form of a modulated wave train:

$$w(\mathbf{x}, t) = \mathrm{Re}\left(e^{i\varphi_0} \int_{-\infty}^{+\infty} \exp\left[-\frac{1}{2}\langle \mathbf{BK}, \mathbf{K}\rangle - i\langle \mathbf{K}, \mathbf{X}\rangle \right] d\mathbf{K} \right), \tag{A8}$$

where the phase of the carrier wave is

$$\varphi_0 = \mathbf{k}_0 \mathbf{x} - \omega_0 t, \tag{A9}$$

and the dimensionless wave vector $\mathbf{K}$ and coordinate $\mathbf{X}$ that characterize small deviations from the carrier wave wave vector $\mathbf{k}_0$ and its trajectory in the coordinate space are

$$\mathbf{K} = (\kappa_x/\Delta k,\ \kappa_y/\Delta l), \quad \mathbf{X} = (\Delta k(x - \omega'_k \mid_{\mathbf{k}=\mathbf{k}_0} t), \quad \Delta l(y - \omega'_l \mid_{\mathbf{k}=\mathbf{k}_0} t). \tag{A10}$$

The modulation function given by the Fourier integral in Eq. (A8) is determined by the quadratic form with the dimensionless matrix

$$\mathbf{B} = \begin{bmatrix} (1 + \mathrm{i}t\,\mu_x) & \mathrm{i}t\,\mu_{xy} \\ \mathrm{i}t\,\mu_{xy} & (1 + \mathrm{i}t\,\mu_y) \end{bmatrix}. \tag{A11}$$

The integral in Eq. (A8) can be evaluated explicitly resulting in Ref. [37]:

$$\int_{-\infty}^{+\infty} \exp\left[-\frac{1}{2}\langle \mathbf{BK}, \mathbf{K}\rangle - i\langle \mathbf{K}, \mathbf{X}\rangle \right] d\mathbf{K} = \frac{2\pi}{[\det(\mathbf{B})]^{1/2}} \exp\left[-\frac{\langle \mathbf{B}^{-1}\mathbf{X}, \mathbf{X}\rangle}{2} \right]. \tag{A12}$$

The real part of the matrix $\mathbf{B}$ is positively determined ensuring convergence of the integral (A8) and existence of the inverse matrix $\mathbf{B}^{-1}$. The determinant of the matrix $\mathbf{B}$ is determined through the expression:

$$\Lambda^2 \equiv |\det(\mathbf{B})|^2 = \left\{ \left[1 + t^2\left(\mu_{xy}^2 - \mu_x\mu_y\right) \right]^2 + t^2(\mu_x + \mu_y)^2 \right\}. \tag{A13}$$

As one can see, Λ does not vanish for any dispersion relation $\omega(\mathbf{k})$ and, therefore, the problem of wave caustics never appears within this approach as it generally occurs in the lowest orders of widely used stationary phase or steepest descent methods.

Finally, the reference solution can be written as follows:

$$w(\mathbf{x}, t) = \frac{1}{\sqrt{\Lambda(\mathbf{k}_0, t)}} \exp\left[-\frac{\Phi^2(\mathbf{k}_0, \mathbf{X}, t)}{2\Lambda^2} \right] \cos\left[\varphi_0(\mathbf{k}_0, \mathbf{x}, t) + \varphi_1(\mathbf{k}_0, t) + \varphi_2(\mathbf{k}_0, \mathbf{X}, t) \right]. \tag{A14}$$

We have used here "mixed" notations introducing "fast" $\mathbf{x}$ and "slow" $\mathbf{X}$ variables (A10) in Eq. (A14) to separate dependence on the wave train carrier parameters ("fast" variable $\mathbf{x}$) and transformation of the wave packet shape associated with small deviations from the carrier harmonic wave $\mathbf{k}_0$ ('slow' variable $\mathbf{X}$).

In addition to the carrier wave phase φ_0 (A8), two other phase shifts φ_1 and φ_2 appear in Eq. (A14). The first one φ_1 shifts phases of all wavetrain components by the same value

$$\varphi_1(\mathbf{k}_0, t) = -\frac{1}{2} \arctan\left[\frac{t(\mu_x + \mu_y)}{1 + t^2\left(\mu_{xy}^2 - \mu_x\mu_y\right)} \right]. \tag{A15}$$

In general, the phase $\varphi_1(\mathbf{k}_0, t)$ decays with time as t^{-1} being dependent on signatures of the second differentials $\mu_x,\ \mu_y,\ \mu_{xy}$. For the isotropic case and in the special case of $\mu_{xy}^2 - \mu_x\mu_y = 0$ (see Ref. [18]), φ_1 converges to the well-known result of the Stationary Phase Method $\varphi_1 = \pm\pi/4$ (see, e.g., Ref. [37]).

The phase shift $\varphi_2(\mathbf{X}, \mathbf{k}_0, t)$ depends on both the wavetrain dispersion parameters and "slow" coordinate $\mathbf{X} = (X_1, X_2)$:

$$\varphi_2(\mathbf{X}, \mathbf{k}_0, t) = \frac{1}{2D^2}\{X_1^2[t^3\mu_y(\mu_{xy}^2 - \mu_x\mu_y) - t\mu_x] + X_2^2[t^3\mu_x(\mu_{xy}^2 - \mu_x\mu_y) - t\mu_y]$$
$$-2X_1X_2t\mu_{xy}[1 + t^2(\mu_{xy}^2 - \mu_x\mu_y)]\}. \quad \text{(A16)}$$

This phase addition vanishes for the wavetrain carrier harmonic ($\mathbf{X} = 0$) and changes peripheral harmonics when $\mathbf{X} \neq 0$. For deep water waves at $t \to +\infty$ the lines of constant phases of Eq. (A16) are hyperbolas, and the phase $\varphi_2(\mathbf{X}, \mathbf{k}, t)$ decays as t^{-1}.

The argument of the exponential function in Eq. (A14) preserves the Gaussian shape of the wave train modulation. The isolines of $\Phi(\mathbf{k}_0, \mathbf{X}, t)$ are ellipses:

$$\Phi(\mathbf{k}_0, \mathbf{X}, t) = X_1^2[1 + t^2(\mu_{xy}^2 + \mu_y^2)] + X_2^2[1 + t^2(\mu_{xy}^2 + \mu_x^2)] - 2X_1X_2t^2\mu_{xy}(\mu_x + \mu_y), \quad \text{(A17)}$$

whose parameters (orientation and eccentricity) vary with time. Equation (A17) can be rewritten in the following form:

$$\Phi(\mathbf{k}_0, \mathbf{X}, t) = -t^2[(X_1\mu_{xy} - X_2\mu_x)^2 + (X_2\mu_{xy} - X_1\mu_y)^2] - X_1^2 - X_2^2, \quad \text{(A18)}$$

which clearly illustrates the effects of the wave packet rotation and stretching from the initial state $X_1^2 + X_2^2 = \text{const}_1$ to asymptotic one ($t \to +\infty$) when $(X_1\mu_{xy} - X_2\mu_x)^2 + (X_2\mu_{xy} - X_1\mu_y)^2 = \text{const}_2$. It should be stressed that isotropy of the initial distribution and/or of dispersion relation does not cancel these effects (see Fig. 2 and comments in Ref. [18]).

The factor D affects the wavetrain modulation in two ways (A14): the magnitude of perturbation decays but its width in coordinate space grows to preserve the total energy. In general, when the dispersion factor does not vanish, i.e., $(\Omega''_{kl})^2 - \Omega''_{kk}\Omega''_{ll} \neq 0$ ($\mu_{xy}^2 - \mu_x\mu_y \neq 0$), the wave train in two-dimensional space decays as t^{-1}. In the special case of "quasi-dispersion," $(\Omega''_{kl})^2 - \Omega''_{kk}\Omega''_{ll} = 0$, the decay becomes slower and follows the one-dimensional asymptotics $t^{-1/2}$.

Thus, the RSA described here reproduces the well-known results of the stationary phase method. Moreover, it allows for the realization of Kelvin's idea [35] "to smooth, to smear" formally infinite growth at wave caustics in a consistent way. Meanwhile, it is not a general method of solution of an arbitrary initial (boundary) value problem. The issues of completeness and uniqueness of the solutions are beyond the scope of this paper. An important point to emphasize is that the method is multidimensional. Therefore, it essentially extends similar results for one-dimensional waves [47] and captures new physical effects like the wave packet rotation.

[1] W. Thomson, XLII. On stationary waves in flowing water. Part I, Philos. Mag. Ser. 5 **22**, 353 (1886).
[2] H. Lamb, *Hydrodynamics*, 6th ed. (Cambridge University Press, Cambridge, England, 1978).
[3] J. Lighthill, *Waves in Fluids* (Cambridge University Press, Cambridge, UK, 1978), p. 504.
[4] L. N. Sretenskii, *The Theory of Wave Motion of Fluid*, 2nd ed. (in Russian) (Nauka, Moscow, 1977).
[5] G. B. Whitham, *Linear and Nonlinear Waves* (Wiley, New York, 1974), p. 636.
[6] M. Kashiwagi, Transient responses of a VLFS during landing and take-off an airplane, J. Mar. Sci. Technol. **9**, 14 (2004).
[7] J. W. Davys, R. J. Hosking, and A. D. Sneyd, Waves due to a steadily moving source on a floating ice plate, J. Fluid Mech. **158**, 269 (1985).
[8] E. Dinvay, and H. Kalisch, and E. I. Părău, Fully dispersive models for moving loads on ice sheets, J. Fluid Mech. **876**, 122 (2019).
[9] K. Johnsen, H. Kalisch, and E. I. Părău, Ship wave patterns on floating ice sheets, Sci. Rep. **12**, 18931 (2022).

[10] W. S. Nugroho, K. Wang, R. J. Hosking, and F. Milinazzo, Time-dependent response of a floating flexible plate to an impulsively started steadily moving load, J. Fluid Mech. **381**, 337 (1999).

[11] A. V. Pogorelova, V. M. Kozin, and A. A. Matyushina, Stress-strain state of ice cover during aircraft takeoff and landing, J. Appl. Mech. Tech. Phys. **56**, 920 (2015).

[12] V. A. Squire, R. J. Hosking, A. D. Kerr, and P. J. Langhorne, *Moving Loads on Ice Plates*, Solid Mechanics and Its Applications (Kluwer Academic Publishers, Dordrecht, 1996).

[13] I. V. Sturova, Unsteady three-dimensional sources in deep water with an elastic cover and their applications, J. Fluid Mech. **730**, 392 (2013).

[14] I. V. Sturova, The effect of non-uniform compression of an elastic plate floating on the fluid surface on the development of unsteady flexural-gravity waves, Fluid Dyn. **56**, 211 (2021).

[15] I. V. Sturova, Motion of a load over an ice sheet with non-uniform compression, Fluid Dyn. **56**, 503 (2021).

[16] A. E. Bukatov, *Waves in Sea with Floating Ice Cover* (Marine Hydrophysical Institute of RAS, Sebastopol, Russia, 2017).

[17] M. J. Lighthill, Contributions to the theory of waves in nonlinear dispersive systems, J. Inst. Maths. Appl. **1**, 269 (1965).

[18] V. G. Gnevyshev and S. I. Badulin, On the asymptotics of multidimensional linear wave packets: Reference solutions, Moscow Univ. Phys. Bull. **72**, 415 (2017).

[19] V. G. Gnevyshev and S. I. Badulin, On reference solutions for ship waves, AIP Adv. **10**, 025014 (2020).

[20] V. Gnevyshev and S. Badulin, Wave patterns of gravity-capillary waves from moving localized sources, Fluids **5**, 219 (2020).

[21] V. Gnevyshev and S. Badulin, Deep water waves from oscillating elliptic source, Water Waves **5**, 239 (2023).

[22] H. Liang and X. Chen, Asymptotic analysis of capillary-gravity waves generated by a moving disturbance, Eur. J. Mech. B Fluids **72**, 624 (2018).

[23] F. Moisy and M. Rabaud, Mach-like capillary-gravity wakes, Phys. Rev. E **90**, 023009 (2014).

[24] F. Noblesse, J. He, Y. Zhu, L. Hong, C. Zhang, R. Zhu, and C. Yang, Why can ship wakes appear narrower than Kelvin's angle? Eur. J. Mech. B/Fluids **46**, 164 (2014).

[25] G. Rousseaux and H. Kellay, Classical hydrodynamics for analogue spacetimes: Open channel flows and thin films, Philos. Trans. R. Soc. A **378**, 20190233 (2020).

[26] P. N. Svirkunov and M. V. Kalashnik, Phase patterns of dispersive waves from moving localized sources, Phys.-Usp. **57**, 80 (2014).

[27] L. Rayleigh, The form of standing waves on the surface of running water, Proc. London Math. Soc. **s1-15**, 69 (1883).

[28] G. G. Stokes, in *1905 Mathematical and Physical Papers* (Cambridge University Press, Cambridge, reprinted by Johnson Reprint Co., New York, 1966), Vol. 5, pp. 362–368.

[29] G. D. Crapper, Surface waves generated by a travelling pressure point, Proc. Roy. Soc. A **282**, 547 (1964).

[30] Z. F. Li, G. X. Wu, and Y. Y. Shi, Wave motions due to a point source pulsating and advancing at forward speed parallel to a semi-infinite ice sheet, Phys. Rev. Fluids **9**, 014801 (2024).

[31] Y. A. Stepanyants and I. V. Sturova, Waves on a compressed floating ice plate caused by motion of a dipole in water, J. Fluid Mech. **907**, A7 (2021).

[32] F. Milinazzo, M. Shinbrot, and N. W. Evans, A mathematical analysis of the steady response of floating ice to the uniform motion of a rectangular load, J. Fluid Mech. **287**, 173 (1995).

[33] W. F. Weeks and D. L. Anderson, An experimental study of strength of young sea ice, Trans. Amer. Geophys. Union **39**, 641 (1958).

[34] A. G. Voronovich, Propagation of internal and surface gravity waves in the approximation of geometrical optics, Izv. Acad. Sc. USSR. Atm. Ocean. Phys. **12**, 850 (1976).

[35] L. Kelvin, Deep sea ship waves, Proc. Roy. Soc. Edinburgh **25**, 1060 (1906).

[36] M. Rabaud and F. Moisy, Ship wakes: Kelvin or Mach angle? Phys. Rev. Lett. **110**, 214503 (2013).

[37] M. V. Fedoryuk, *Saddle Point Method*, Encyclopedia of Mathematics (EMS Press, Berlin, 2001).

[38] M. Benzaquen, A. Darmon, and E. Raphael, Wake pattern and wave resistance for anisotropic moving disturbances, Phys. Fluids **26**, 092106 (2014).

[39] J. W. Schulkes, R. J. Hosking, and A. D. Sneyd, Waves due to a steadily moving source on a floating ice plate. Part 2, J. Fluid Mech. **180**, 297 (1987).

[40] J. W. Schulkes and A. D. Sneyd, Time-dependent response of floating ice to a steadily moving load, J. Fluid Mech. **186**, 25 (1988).

[41] V. V. Bulatov and I. Yu. Vladimirov, Far fields at interface between an infinitely deep ocean and ice excited by a localized source, Izv. Atmos. Ocean. Phys. **59**, 296 (2023).

[42] V. V. Bulatov, I. Yu. Vladimirov, and E. M. Morozov, Perturbations far fields of the interface surface of the deep ocean and the ice cover from localized sources, Doklady Russ. Acad. Sci., Earth Sciences. **512**, 302 (2023).

[43] Zh. V. Malenko and A. A. Yaroshenko, Three-dimensional bending-gravitational waves in a floating ice sheet from a moving source of disturbances, Prikl. Matemat. Mehan. (J. Appl. Math. Mech.) **87**, 1037 (2023).

[44] Zh. V. Malenko and A. A. Yaroshenko, Flexural-gravity waves in an ice cover exited by periodically varying moving perturbations, Fluid Dynamics **59**, 415 (2024).

[45] V. V. Bulatov and I. Yu. Vladimirov, The phase structure of wave disturbances excited by a pulsating source at the interface of a liquid flow of finite depth and an ice sheet, Prikl. Matemat. Mehan. (J. Appl. Math. Mech.) **88**, 392 (2024).

[46] L. A. Tkacheva, Motion of a load on an ice cover in the presence of a current with velocity shear, Fluid Dyn. **58**, 263 (2023).

[47] G. F. Clauss and J. Bergmann, Gaussian wave packets—A new approach to seakeeping tests of ocean structures, Appl. Ocean Res. **8**, 190 (1986).